Derivation of Spatially Distributed Thermal Comfort Levels in Jordan as Investigated From Remote Sensing, GIS Tools and Computational Methods

ibrahim M. oroud (✉ ioroud@mutah.edu.jo)

Mu'tah University

Derivation of spatially distributed thermal comfort levels in Jordan as investigated from remote

sensing, GIS tools and computational methods

Ibrahim M. Oroud

Mu'tah University

Jordan

ioroud@mutah.edu.jo

1   Derivation of spatially distributed thermal comfort levels in Jordan as investigated from remote

2   sensing, GIS tools and computational methods

3   Abstract

4   Thermal comfort is usually calculated using discrete point measurements. This procedure is not

5   suitable to study thermal comfort for inhabited areas with rugged terrains where climate gradient is

6   high. The wide availability of remote sensing data and GIS tools have revolutionized data management,

7   processing and visualization. The present paper implemented digital elevation data, GIS tools and a

8   computational algorithm to generate spatially continuous maps of climatological elements which were

9   employed to derive thermal comfort levels across Jordan. Results show detailed information of the

10   spatial distribution of the degree of thermal comfort in winter and summer across the country which

11   cannot be resolved using discrete point measurements. It is shown that the mountainous areas in the

12   country, where most urban centers are situated, experience "slightly warm" to "warm" indoor apparent

13   temperatures in summer. The Jordan Valley and the desert experience high indoor apparent

14   temperatures in summer. Cold conditions prevail over most parts of the country, with the heating

15   degree days ranging from 2100 in the southern mountains to values close to zero near the Dead Sea

16   area. The presented procedure demonstrated that the very low levels of ambient vapor pressure is an

17   important atmospheric forcing contributing to the widespread cold conditions prevailing over the desert

18   areas in winter. The efficiency of direct evaporative cooling systems to achieve thermal comfort in the

19   various parts of the country is investigated. The procedure presented can be used over regional scales

20   with different levels of spatial resolutions for a wide range of climatological studies.

21   Keywords: big data, thermal comfort, spatially distributed maps, evaporative cooling, climate data,

22   Jordan

23   1- Introduction

24   Thermal comfort is a bioclimatic indicator reflecting the level of thermal comfort/discomfort within a

25   climate regime during a specific period of time. The American Society of Heating, Refrigerating and Air-

26   Conditioning Engineers (ASHRAE, 2009) defines thermal comfort as "the condition of mind that expresses

27   satisfaction with the thermal environment and is assessed by subjective evaluation" (Fergus, 2001).

28   Energy consumption, outdoor working conditions, recreational activities, environmental tourism and

29   many other economic activities are strongly influenced by the level of thermal comfort (De Dear and

30 Brager, 2002; Humphreys and Fergus, 2000; Orosa, 2009). Thermal comfort index can be used to

31 estimate energy demands needed for heating and cooling purposes during the annual cycle.

32 Unusual weather conditions could pose a threat to human lives. For instance, high temperatures and

33 elevated humidity have been reported to increase hospitalization and death rates among vulnerable age

34 group (Anderson et al. 2013; Basu et al. 2010). The scenarios of increased air temperature caused by

35 global warming could exacerbate thermal discomfort in many regions across the globe, rendering living

36 conditions rather very difficult or very expensive (Marx et al. 2021; Mistry, 2020). There is an

37 increased risk of more frequent heat waves following a climate change (Meehl and Tebaldi 2004). Ill

38 health and mortality rate are endangered by temperatures outside the thermal comfort range.

39 Physiological, psychological and environmental parameters such as metabolic heat generation, age,

40 clothing, mean radiant temperature, ambient relative humidity, airflow rate and heat gain from

41 radiation source work hand in hand to influence the perception and degree of thermal comfort

42 (Steadman, 1979a,b; Schweikera et al., 2017). Thermal comfort is usually assessed using point

43 measurements due usually to the limited number of observational sites and the ease to generalize

44 results (Fang et et al., 2004; Fang; Oliveira and Andrade, 2007; Orimoloye et al., 2017). Spatially

45 continuous thermal comfort levels were derived for global or continental scales (Matzarakis and

46 Amelung, 2008; Mistry, 2020; Yan et al., 2021). These representations are useful to develop a general

47 idea of thermal comfort over different geographic zones. Due to their very coarse spatial resolutions,

48 these procedures cannot be used for operational purposes, particularly in areas with rugged terrains.

49 The increased capabilities of computational power along with the availability of fine resolution

50 spatially gridded elevation data and the interpolation capabilities of GIS tools have revolutionized data

51 management, and thus large volumes of data could be generated, processed, and visualized across

52 regional scales. Thus, the objective of the present investigation is to derive spatially continuous thermal

53 comfort levels across Jordan using digital elevation data, GIS tools and limited meteorological data.

54 The generated maps provide objective means to identify the spatial distribution of thermal comfort

55 across the study area. The procedure could be extended to evaluate energy demands for heating and

56 cooling purposes, suitability of different areas for evaporative cooling and to locate suitable sites for

57 recreational activities and other tourism purposes.

58 2- Study area

59 The present procedure is applied to the country of Jordan. Jordan extends from 29.19^O to 33.35^O N and

60 from 34.95^O to 39.3^O E, with a total surface area of ~90000 km^2 (Figure 1). The study area spans wide

61 topographic variations, with the elevation ranging from 250- 436 m below mean sea level near the

62 Dead Sea area and along the Jordan Valley to more than 1700 m in the southern mountains. There is a

63 steep elevation gradient across the east-west direction, and as a result, a steep climate gradient exists

64 across the east-west and in the north- south directions. Figure 2 shows the topography of the study area.

65 Precipitation in this area ranges from a few mm/year in southeastern Jordan to about 600 mm/year in a

66 small enclave in the northwestern part of the country. Air temperature depends on the elevation and

67 longitude, with the average annual temperature ranging from 26.5 ^{O}C near the southern Dead Sea to

68 about 14 ^{O}C in the southern mountains.

69 3. Method of investigation

70 3.1 Remote Sensing data and GIS tools

71 Digital elevation data (DEM) were downloaded from the Shuttle Radar Topographic Mission (SRTM)

72 from the USGS site. The DEM data have a geographic coordinate system and a spatial resolution of

73 one arc second ($\approx$ 30 m). The DEM image was reprojected to the UTM coordinate system, zone 36 to

74 allow proper computation of distances across the grids. To facilitate processing of this very large

75 dataset, the DEM data were resampled to one km spatial resolution. Arc Map (version 10.7) was used

76 to extract the coordinates and elevation of each grid point. Generated coordinates and elevation for

77 each grid were exported to a csv file for further processing by the numerical model. Figure 3 presents a

78 flow chart of method used in this investigation.

79 3.2- Climatological data

80 Meteorological stations in Jordan are relatively sparse and poorly distributed, and thus climate

81 elements over large parts of the country are not monitored, rendering these area as "blind spots".

82 Twenty-two meteorological stations were used to carry out the calculation of the thermal comfort

83 index. The average monthly temperature and relative humidity for the meteorological stations were

84 obtained from the Department of Meteorology, Jordan. Table 1 shows the coordinates, elevation,

85 average monthly air temperature and relative humidity of the stations used in this investigation. To

86 improve the integrity of the model and provide a better representation of the study area, five additional

87 stations were synthetically generated. This was done primarily along the Dead Sea and in Wadi Araba

88 due to the scarcity of measuring stations. The temperature and relative humidity of each synthetic

89   station were derived based on field measurements and a few other criteria including its elevation, the

90   general climate pattern of the nearest measuring stations, wind regime and energy balance

91   considerations (Oroud, 1997).

92   3.3 Numerical procedure

93   Interpolation by GIS tools is purely spatial, and thus climate gradient induced by elevation differences

94   across a landscape is usually masked out. The problem of GIS interpolation can become severe if

95   weather measuring stations are sparsely distributed over very rugged terrains (e.g., Jeffrey et al., 2001;

96   Apaydin et al., 2004). In this case direct interpolation techniques in the GIS environment do not

97   produce adequate results, and large deviations may result. Under such conditions, a better procedure to

98   generate accurate data between measuring sites would be to build a numerical procedure which takes

99   into account the neighboring measuring sites along with vertical and horizontal gradient of the intended

100   climate elements across the landscape. The computational procedure provides an explicit algorithm to

101   calculate meteorological elements at each grid point. This procedure produces a dense point network

102   which enables GIS to produce accurate spatially distributed raster database.

103   Two steps are needed to generate climatological data over a spatial grid. The one is obtaining the

104   distance between the grid and measuring sites, and the second one is calculating the climatological

105   element using the closest n stations after taking into account the elevation difference between each

106   measuring site and the spatial grid.

107   The Euclidean distance between grid j and a measuring site is computed as,

108
$$\delta_{i,k} = \sqrt{(x_i - x_j)^2 + (y_i - y_j)^2} \tag{1}$$

109

110   where $\delta_{i,k}$ is the Euclidean distance (m) between station i and the intended grid cell, and the x and y are

111   the easting and northing coordinates (m).

112   The temperature of each grid ($T(x_k,y_k,z_k)$) was calculated explicitly using the inverse distance weighting

113   procedure (IDW) using the following equation (Emmendorfer and Dimuro, 2020),

114
$$T(x_k, y_k, z_k) = \sum_{i=1}^{j}(Ti + \Gamma(zi - z(k))/\delta(i,k)^2 /(\sum_{i=1}^{j}\frac{1}{\delta(i,k)^2}) \tag{2}$$

115   where x_k is the easting (m), y_k is the northing (m) and z_k is the elevation of the grid; T_i is the

116   temperature of station i, Γ is the environmental lapse rate (${}^{o}C\ m^{-1}$), z_i is the elevation of station i, z(k) is

117 the elevation of the grid, and δ(i,k) is the Euclidean distance between station i and the intended cell. In

118 this procedure, the closest three stations were chosen to carry out the interpolation of temperature for

119 each grid (the j parameter in Eqn. 2).

120
$$\delta(i,k) = \min(\delta_i, \delta_{i+1}, ..., \delta_n) \tag{3}$$

121 The actual vapor pressure is computed from the interpolated relative humidity and saturation water

122 vapor pressure at each grid,

123
$$e_a = RH \times e_s \tag{4}$$

124 where RH is the relative humidity (%), e_a and e_s are the actual and saturated vapor pressure (kPa),

125 respectively. The saturation vapor pressure at a grid is calculated using the following form (Oroud,

126 2011),

127
$$e_s = 0.61078 \, exp(\frac{17.269T}{(237.3+T)}) \tag{5}$$

128 Where T is the grid temperature (°C).

129 The wet bulb temperature which is an important indicator of the evaporating power of air is usually

130 used to assess the efficiency of using evaporative cooling systems. The wet bulb temperature is

131 calculated for each grid from air temperature and relative humidity of the interpolated grid using the

132 procedure presented by Stull (2011) expressed as,

133 $WBT = T_a + atan\sqrt{(0.151977 \times (RH + 8.313659))}$+ atan(T$_a$+RH)-atan(RH-

134 $1.67633)+0.00391838 \times RH^{1.5} \times atan\,(0.023101 \times RH))-4.686035$ *(6)*

135 where WBT is the wetbulb temperature, Ta is air temperature, $atan$ is the arctangent of the expression

136 expressed in radian, and RH is the relative humidity (%).

137 3.4 Thermal comfort index

138 Numerous methods have been suggested in the literature to provide a quantitative metric to gauge

139 thermal comfort (Anderson et al., 2013; Brager et al., 1998). The most accurate method would be to

140 use a detailed energy budget equation in which heat gain and loss from the human subject are taken

141 into account (Fang et al., 2004; Orosa, 2009; Steadman, 1984). Because of the complex nature of

142 thermal comfort due to the many environmental, physiological and psychological factors involved,

143 simple empirical equations have been developed to provide an approximate representation of the level

144 of thermal comfort/discomfort in indoor and outdoor conditions (Fabbri, 2015; Steadman, 1979a,b).

145   Thermal comfort for unconditioned buildings is controlled by meteorological elements of the outside

146   environment. De Dear and Brager (2002), Humphreys and Fergus (2000) indicated a close link

147   between the effective temperature of unconditioned buildings and outdoor air temperature. In many

148   third world countries, buildings are not air conditioned due to lack of financial resources required to

149   achieve thermal comfort, and thus thermal comfort of these dwellings respond directly to outdoor

150   meteorological conditions.

151   Numerous thermal comfort indices exist in the literature such as the heat index, humidex, wet-bulb

152   globe temperature, apparent temperature (Fabbri, 2015; Orosa, 2009; Orimoloye et al., 2017; Tseliou et

153   al., 2010). Most indices use air temperature and a psychrometric variant- e.g., relative humidity,

154   ambient vapor pressure, dew point or wet bulb temperature (ASHRAE, 2009; Anderson et al., 2013).

155   Some indices use additional environmental variables such as wind speed and solar radiation. The major

156   differences among most indices are in the empirical coefficients used in each algorithm. Anderson et al

157   (2013) compared 21 thermal index algorithms and concluded that most of them generate values which

158   are consistent with the apparent temperature as presented by Steadman (1978 a, b). Detailed

159   discussions of the various thermal indices and methods to calculate each of them was presented by

160   numerous authors (e.g., Anderson et al., 2013; Blazejczyk et al., 2010; Mistry, 2020).

161   The elegance of algorithms using air temperature and humidity is their simplicity and the wide

162   availability of required parameters. Popular thermal indices which use only air temperature and a

163   humidity element include the Discomfort Index, the temperature-humidity Index, the Humidex, and the

164   Ambient Indoor Index (e.g., Orimoloye et al., 2017; Yan et al., 2021). The Discomfort Index (DI), the

165   indoor apparent temperature (IAT), the Temperature- Humidity Index (THI) and the Humidex may be

166   respectively written using the following form (Anderson et al., 2013),

167    $$DI = 8.3 + 0.4\,(WBT + T_a)\qquad\qquad(7)$$

168    $$IAT = -1.3 + 0.92 T_a + 0.22\,e_a\qquad\qquad(8)$$

169    $$THI = T_a - (0.55 - 0.0055\,RH)(T_a - 14.44)\quad(9)$$

170    $$Humidex = T_a + 0.555(e_a - 10)\qquad\qquad(10)$$

171   where WBT is the wet bulb temperature ^{O}C, e_a is the ambient vapor pressure in hPa, T_a is the ambient

172   air temperature ^{O}C, and RH is the relative humidity of air in %. The apparent indoor temperature and

173   the temperature humidity index can be used during the different seasons. In this investigation, the IAT

174   is chosen to calculate thermal comfort because it can be calculated for a wide range of ambient

175   conditions and computed values were found to compare favorably well with the Universal Thermal

176   Climate Index (UTCI) (Blazejczyk et al., 2012; Mistry, 2020). Table 2 shows the designation of the

177   thermal comfort categories and corresponding IAT values (Matzarakis and Amelung, 2008)). There is

178   correspondence between the values of these indices and thermal comfort/ human activity. For instance,

179   when the IAT rises above 35, considerable discomfort is common, work efficiency is compromised,

180   and physical activity should be reduced or stopped altogether (Schlatter, 1987).

181   4- Results

182   4.1 Air temperature

183   Outside air temperature is a good indicator of thermal comfort within unconditioned buildings. Figure 4

184   shows the spatial distribution of average monthly air temperature during January and July, respectively.

185   Wide temperature differences are observed across the study area during these two months. A distinct

186   temperature gradient is very clear along the Jordan Valley in both months. For instance, the average

187   temperature in January ranges from ~ 3 $^\circ$C in the high southern mountains to more than 16 $^\circ$C in the

188   Jordan Valley close to the Dead Sea. An important observation for January is the prevalence of low

189   temperatures in the desert areas which cover the eastern and southeastern areas of the country.

190   Although desert areas receive relatively more solar radiation than the mountainous areas during the

191   daytime hours in winter, thermal radiation deficit there is very high during winter due to clear skies and

192   low moisture content in the troposphere.

193   The summer months, as represented by July, display a different spatial temperature distribution pattern

194   compared to January. Unlike winter, desert areas experience high temperatures in summer, and the near

195   surface air temperature of some of these locations rival those along the Jordan Valley despite the

196   significant elevation differences between the Jordan Valley and desert areas. All locations along the

197   Jordan Valley are situated much below sea level- ~250 – 430 m below sea level, whereas the desert

198   landscape has elevations ranging from 550 m to more than 1000 m above mean sea level.

199   4.2 The indoor apparent temperature

200   The spatial distribution of indoor apparent temperature is presented in Figure 5 for January and July as

201   the two endpoints of the annual cycle. The Jordan Valley attains very high IAT values during July, with

202   average values ranging from 30 to more than 36 $^\circ$C. Comfortable conditions during summer are

203   restricted to the southern mountains and a few other highland enclaves in central and northern Jordan.

204   With the exception of weather conditions associated with heat waves, the mountainous areas in Jordan

205   where most urban centers are situated can be classified on average as "slightly warm". The

206   northwestern part of the country and the central part appear on the map as being on the warm side; this

207   is due to low elevation and high vapor pressure content in the atmosphere. A strong indoor temperature

208   gradient exists between the mountains and the desert in the east and southeast. In addition to the large

209   amount of solar radiation reaching their surface, desert surfaces are devoid of vegetation cover,

210   transforming all surface net radiation into subsurface heat storage and sensible heat flux to the

211   contiguous atmosphere (Oroud, 2020). As a result of the strong surface and near surface heating during

212   summer, thermal comfort levels in a large portion of the desert areas are very close to those

213   encountered in the Jordan valley.

214   The spatial distribution of indoor apparent temperature in winter (Figure 5.b) differs drastically from

215   corresponding values in July. With the exception of the Jordan Valley which maintains relatively

216   pleasant thermal comfort levels, most other areas experience cold or very cold conditions during

217   winter. The indoor apparent temperature ranges from very cold as in the southern mountains to cold in

218   the reset of the country. Surprisingly, most of the mountainous areas in northern Jordan experience

219   more amenable thermal comfort levels compared to desert areas in winter. The relatively less harsh

220   thermal conditions in the northern mountains during winter, despite their higher elevations compared to

221   the desert areas, are likely linked to larger soil moisture and the greater probability of cloud cover

222   during the nighttime hours.

223   Although desert areas are relatively hot in summer, cold conditions are widespread during the winter

224   months. Surface thermophysical properties and atmospheric forcings can be cited for the anomalously

225   cold conditions in the desert areas in winter. Desert areas have usually dry coarse bare surfaces which

226   have low thermal conductivity, and thus the layer involved in warming up/cooling processes during the

227   diurnal cycle is rather very shallow, leading to rapid and extensive cooling during the long night hours.

228   Two additional atmospheric factors enhance nighttime cooling- the first one is the usual absence of

229   cloud cover, and the second factor is the low moisture content in the troposphere. Figure 6 shows the

230   spatial distribution of actual vapor pressure across the country. It is clear that desert areas are

231   characterized with very low actual vapor pressure due to lack of soil moisture on the one hand and their

232   remoteness from water bodies. The dewpoint temperature as inferred from Figure 6 is either close to

233   zero or below zero over a large portion of the desert areas. Thus, the very low dewpoint temperatures

234 across the desert in winter explain the widespread cold conditions in this area. A strong correlation

235 exists between thermal comfort and elevation as presented in Figure 7. The correlation coefficient in

236 January is ~0.97 whereas its corresponding value in July and August is ~ 0.92 and 0.93, respectively.

237 Summer has a larger lapse rate than winter, with values of 0.67 ^{O}C/100 m and 0.8 ^{O}C/100 m in January

238 and July/August, respectively.

239 Unlike point measurements which provide information in the immediate vicinity of the measuring site,

240 the present procedure is able to map thermal comfort continuously across a very large, rugged area with

241 substantial climate gradients. This point is evident when inspecting the indoor apparent temperature

242 gradient between the mountains and the Jordan Valley. Furthermore, the present procedure is able to

243 establish a physical link between the widespread cold conditions over the desert and the spatial

244 distribution of actual vapor pressure.

245 4.3 Implications for heating and cooling

246 Results presented in this investigation can be extended to examine the heating and cooling load for any

247 specific location during the course of year. Figure 8 shows the average monthly indoor apparent

248 temperature for twenty-two locations, many of which are situated in or close to major urban centers.

249 This table shows that most areas in Jordan experience cold conditions during winter months and as

250 such require a large investment of energy- fuel/gas/ electricity- to meet heating requirements of

251 occupied buildings like offices and homes. Most locations in Jordan require heating from November to

252 the end of March but with wide variations. This point raises an important issue regarding the wisdom

253 of specifying the beginning of November as the starting date for winter in Jordan. This date implies

254 that public offices are allowed to use heating systems regardless of the location of the building whether

255 it is near the Dead Sea or in the high southern mountains. Results presented in this paper provide some

256 guidelines of the different thermal comfort zones in the country during winter.

257 Heating requirement for each location can be determined roughly from Figure 8. For instance, the

258 heating degree days for a base temperature of 18 ^{O}C may range from ~ 2200-degree days in the

259 southern mountains to 145-degree days near the southern corner of the Dead Sea. Mountainous and

260 desert locations require on average between 1000- 1400- degree days of heating.

261 Cooling is definitely not as demanding as heating in most locations in the country. Cooling may be

262 required in the late afternoon hours in most large urban centers during July, August and September.

263   The Jordan Valley and desert areas require a great deal of energy investment for cooling purposes to

264   bring about thermal comfort.

265   To cutdown on energy spending, direct evaporative cooling systems are usually employed in low-

266   income communities (Basediya et al., 2013; Camargo, 2013). Evaporative cooling systems use only

267   water and a blower to cool unsaturated air when forced through a water-saturated porous medium. The

268   temperature of blown air is cooled down via evaporating water from the saturated medium. This mode

269   is characterized by very low energy consumption compared to refrigerating units. A major factor

270   influencing the use of evaporative cooling for thermal comfort purposes is the wet bulb temperature,

271   which can be used to gauge the efficiency of this cooling mode. Figure 9 displays the spatial

272   distribution of the wet bulb temperature along with the major urban centers. Evaporative cooling

273   systems have an efficiency of 50% to 70% (e.g., Basediya et al., 2013; Camargo, 2013). For instance,

274   the blown air passing a porous saturated medium can be expressed as (Basediya et al., 2013),

275   $$T_{out} = T_{in} - \alpha[T_{in} - T_{wb}] \qquad\qquad (11)$$

276   Where T_{out} is the resulting air temperature after passing through the saturated medium, T_{in} is the blown

277   outside air, α is the efficiency of the cooling system, and T_{wb} is the wet bulb temperature. The

278   efficiency of the cooling system is a measure of how closely the supply air temperature leaving the

279   evaporative cooler approaches the outdoor wet-bulb temperature. A psychrometric chart can be

280   consulted to examine the efficiency of an evaporative cooling system. In general, however, these

281   systems cool the air about 5-7 $^{\circ}$C above the wet bulb temperature. For instance, a midday air

282   temperature of 35 $^{\circ}$C along with a wet bulb temperature of 20 $^{\circ}$C and a system efficiency of 0.6 will

283   deliver an air temperature of 25 $^{\circ}$C. Thus, areas with a wet bulb temperature of 20 $^{\circ}$C or less may use

284   evaporative cooling systems with good results. This includes the mountainous areas and most of the

285   desert. When the wet bulb temperature is above 20 $^{\circ}$C, evaporative cooling systems may be inefficient

286   to bring about adequate thermal comfort. Figure 9 shows that the Jordan Valley, some desert areas and

287   the northwestern part of the country have relatively high wet bulb temperature, rendering evaporative

288   cooling systems in these areas rather inefficient in bringing about adequate thermal comfort.

289   5- Discussion

290   The widespread lack of climatological data in many countries is a major problem facing researchers

291   and planners. These data are prerequisite for successful implementation of many operational projects

292   like construction of dams, assessment of irrigation water needs, estimation of evaporation and

293   evapotranspiration from dams and agricultural fields, evaluation of heating and cooling loads, to name

294   a few. The wide availability of remote sensing data, powerful GIS tools and computational methods

295   have revolutionized data handling, processing and visualization.

296   The present paper implemented a combination of tools to generate high spatial resolution

297   meteorological data across a regional scale. The generated data were extended to derive the spatial

298   distribution of thermal comfort across Jordan as a case study. It was shown that the procedure was able

299   to generate spatially continuous high- resolution maps of climatological elements and infer detailed

300   information about their spatial distribution. It was shown for instance, that the widespread cold

301   conditions across the desert in winter is physically linked to the ambient water vapor pressure. Point

302   measurements represent an important database, given their long record. Point measurements suffer

303   from two major weaknesses, the first one is that they represent their immediate surroundings, and thus

304   measured meteorological elements represent a small area particularly in rugged terrains where climate

305   gradient is very large. The second disadvantage is their very limited number, particularly in third world

306   countries due to logistics and financial constraints. For instance, the major portion of the country of

307   Jordan is not covered by any measuring stations, and thus any planning for a project will be based on

308   intuition or guessing, leading most of the time to flawed outcome.

309   5- Conclusion

310   Thermal comfort for cities and small geographic localities has usually been reported in the literature

311   using point measurements. This type of evaluation is adequate for urban centers encountering similar

312   meteorological forcings across the landscape. Urban area spanning a large topographic gradient will

313   experience very different thermal comfort levels. Urban centers built in mountainous areas represent a

314   prime example, and thus the fine spatial details in meteorological conditions influenced by topographic

315   variations should be resolved adequately. The present paper presents an efficient algorithm to generate

316   a big dataset of climatological elements across a large area. Jordan was used as a case study to

317   demonstrate the efficiency of this procedure. Generated climatological data were used to derive high

318   resolution thermal comfort levels across the country.

319 Statements and Declarations

320 There is no financial or other competing of interests.

321

322 References

323 Anderson GB, Bell ML, Peng RD. 2013. Methods to calculate the heat index as an exposure metric in

324   environmental health research. Environ Health Perspect. 121:1111–1119;

325   http://dx.doi.org/10.1289/ehp.1206273

326 Apaydin, H., Sonmez, F. K., Yildirim, Y. E. (2004) Spatial interpolation techniques for climate data in

327   the GAP region in Turkey, Climate Research, 28: 31–40.

328 ASHRAE (2009) Handbook—Fundamentals. Atlanta: American Society of Heating, Refrigerating and

329   Air-Conditioning Engineers, Inc

330 Basediya, A., Samuel, V., Beera, V., (2013). Evaporative cooling system for storage of fruits and

331   vegetables - a review, J Food Sci Technol., 50(3): 429–442. 10.1007/s13197-011-0311-6

332 Blazejczyk, K., Epstein, Y., Jendritzky, G., Staiger, H., Tinz, B. (2010) Comparison of UTCI to

333   selected thermal indices, Int. J. Biometeorol., 56, 515–535, DOI 10.1007/s00484-011-0453-2

334 Brager, Gail S.; de Dear, Richard J. (1998). "Thermal adaptation in the built environment: a literature

335   review". Energy and Buildings. 27 (1): 83–96, doi:10.1016/S0378-7788(97)00053-4. ISSN 0378-

336   7788.

337 Camargo JR. Evaporative cooling: water for thermal comfort. An Interdisciplinary. *J Applied*

338   *Sci.* 2007;3:51–61.

339 De Dear, R. J., Brager, G. S. (2002). Thermal comfort in naturally ventilated buildings: revisions to

340   ASHRAE Standard 55. Energy and buildings, 34(6), 549-561.

341 Emmendorfer L.R., Dimuro G.P. (2020) A Novel Formulation for Inverse Distance Weighting

342   from Weighted Linear Regression. In: Krzhizhanovskaya V. et al. (eds) Computational

343   Science – ICCS 2020. ICCS 2020. Lecture Notes in Computer Science, vol. 12138. Springer,

344   Cham. https://doi.org/10.1007/978-3-030-50417-5_43

345 Fabbri, K., 2015. A Brief History of Thermal Comfort: From Effective Temperature to Adaptive

346   Thermal Comfort, DOI:10.1007/978-3-319-18651-1_2 (in: Indoor Thermal Comfort Perception).

347 Fang, L; Wyon, DP; Clausen, G; Fanger, PO (2004). "Impact of indoor air temperature and humidity in

348   an office on perceived air quality, SBS symptoms and performance". Indoor Air. 14 Suppl 7: 74–

349   81. doi:10.1111/j.1600-0668.2004.00276.x. PMID 15330775.

350 Fergus, N., 2001. Characterizing occupant behavior in buildings, Proceedings of the Seventh

351   International IBPSA Conference. Rio de Janeiro, Brazil. pp. 1073–1078.

352 Humphreys, M., Nicol, Fergus, 2000. Outdoor Temperature and Indoor Thermal Comfort: Raising the

353   Precision of the Relationship for the 1998 ASHRAE Database of Field Studies, ASHRAE

354   Symposia, publication/284652345.

355 Jeffrey, S., Carter, J., Moodie, K., Beswick, A (2001). Using spatial interpolation to construct a

356   comprehensive archive of Australian climate data, Environmental Modelling and Software, 16,

357   309–330.

358 Matzarakis A., Amelung, B (2008) Physiological Equivalent Temperature as Indicator for Impacts of

359   Climate Change on Thermal Comfort of Humans, in M.C. Thomson et al. (eds.), Seasonal

360   Forecasts, Climatic Change and Human Health, Springer Science.

361 Mazinyo, S., Nel, W., Iortyom, E., (2017). Climate Variability and Heat Stress Index have Increasing

362   Potential Ill-health and Environmental Impacts in the East London, South Africa, International

363   Journal of Applied Engineering Research, 12, (17), 6910-6918.

364 Marx W., Haunschild R, Bornmann L. (2021) Heat waves: a hot topic in climate change research.,

365   Theor. Appl. Climatol. 2021 Sep 3:1-20. doi:10.1007/s00704-021-03758-y.

366 Mistry, M. (2020). A high spatiotemporal resolution global gridded dataset of historical human

367   discomfort indices, Atmosphere 2020, 11, 835; doi:10.3390/atmos11080835

368 Orimoloye, I., Mazinyo, S., Nel, W., Iortyom E. (2017) Climate Variability and Heat Stress Index have

369   Increasing Potential Ill-health and Environmental Impacts in the East London, South Africa,

370   International Journal of Applied Engineering Research, 12, 6910-6918

371 Oliveira, S., Andrade, H. (2007) An initial assessment of the bioclimatic comfort in an outdoor public

372   space in Lisbon, Int. J. Biometeorol., 52:69–84, doi: 10.1007/s00484-007-0100-0

373 Orosa, J. A., 2009. On the Origins of Thermal Comfort, European Journal of Scientific Research, 34

374   (4), 561-567.

375 Oroud, IM (1997). Diurnal Evaporation from fresh and hypersaline shallow ponds in a hot, dry

376 environment. *Physical Geography. 18*, no. 4, 363- 382.

377 Oroud, IM (2011). Evaporation from the Dead Sea and its implications on its water balance,

378 *Theoretical and Applied Climatology,* DO1 10.1007/S00704-0452-6*.*

379 Schlatter T.W. (1987) Temperature-humidity index. In: Climatology. Encyclopedia of Earth

380 Science. Springer, Boston, MA. doi.org/10.1007/0-387- Mistry, M. (2020). A high

381 spatiotemporal resolution global gridded dataset of historical human discomfort indices,

382 Atmosphere 2020, 11, 835; doi:10.3390/atmos1108083530749-4_176

383 Schweiker, M., Fuchs, X., Becker, S., Shukuya, M., Dovjak, M., Hawighorst, M., Kolarik, J (2017)

384 Challenging the assumptions for thermal sensation scales, Building Research and Information,

385 45:5, 572-589, DOI: 10.1080/09613218.2016.1183185

386 Steadman, R. G (1979). "The Assessment of Sultriness. Part I: A Temperature-Humidity Index Based

387 on Human Physiology and Clothing Science". J. Appl. Meteorol. 18 (7): 861-873. doi:

388 10.1175/1520-04501.

389 Steadman, R. G. (y 1979). "The Assessment of Sultriness. Part II: Effects of Wind, Extra Radiation and

390 Barometric Pressure on Apparent Temperature". Journal of Applied Meteorology. 18 (7): 874–

391 85, doi:10.1175/1520-04502.

392 Steadman, R. G. (y 11984). A universal scale of apparent temperature, J. Climate A.M, 23, 1674- 1687.

393 Stull, R. (2011) Wet-Bulb Temperature from Relative Humidity and Air Temperature. J. Appl.

394 Meteorol. Climatol., 50, 2267–2269.

395 Tseliou, A., Tsiros, I., Lykoudis, S, Nikolopoulou, M. (2010) An evaluation of three biometeorological

396 indices for human thermal comfort in urban outdoor areas under real climatic conditions, Building

397 and Environment 45 (2010) 1346–1352, doi:10.1016/j.buildenv.2009.11.009

398 Yan, Y., Xu, Y., Yue, S. (2021) A high-spatial-resolution dataset of human thermal stress indices over

399 South and East Asia, Scientific Data, 1 (8), 229, 10.1038/s41597-021-01010-w

400

401   List of Figures

402   Figure 1. Location of the study area.

403   Figure 2. Topography of study area along with the measuring climatological stations.

404   Figure 3. Flowchart of steps used to carry out the investigation.

405   Figure 4. The spatial distribution of average monthly air temperature in July and January.

406   Figure 5. The spatial distribution of indoor apparent temperature in July and January.

407   Figure 6. The spatial distribution of ambient vapor pressure across Jordan in January.

408   Figure 7. A scatterplot of the relationship between indoor thermal comfort and elevation.

409   Figure 8. The average monthly indoor apparent temperature for twenty-two locations.

410   Figure 9. Spatial distribution of the wet bulb temperature during July.

411

412

413   List of Tables

414   1-   Table 1. Meteorological stations along with their geographic and climatological properties

415   2-   Table 2. The designation of the thermal comfort categories and corresponding IAT values
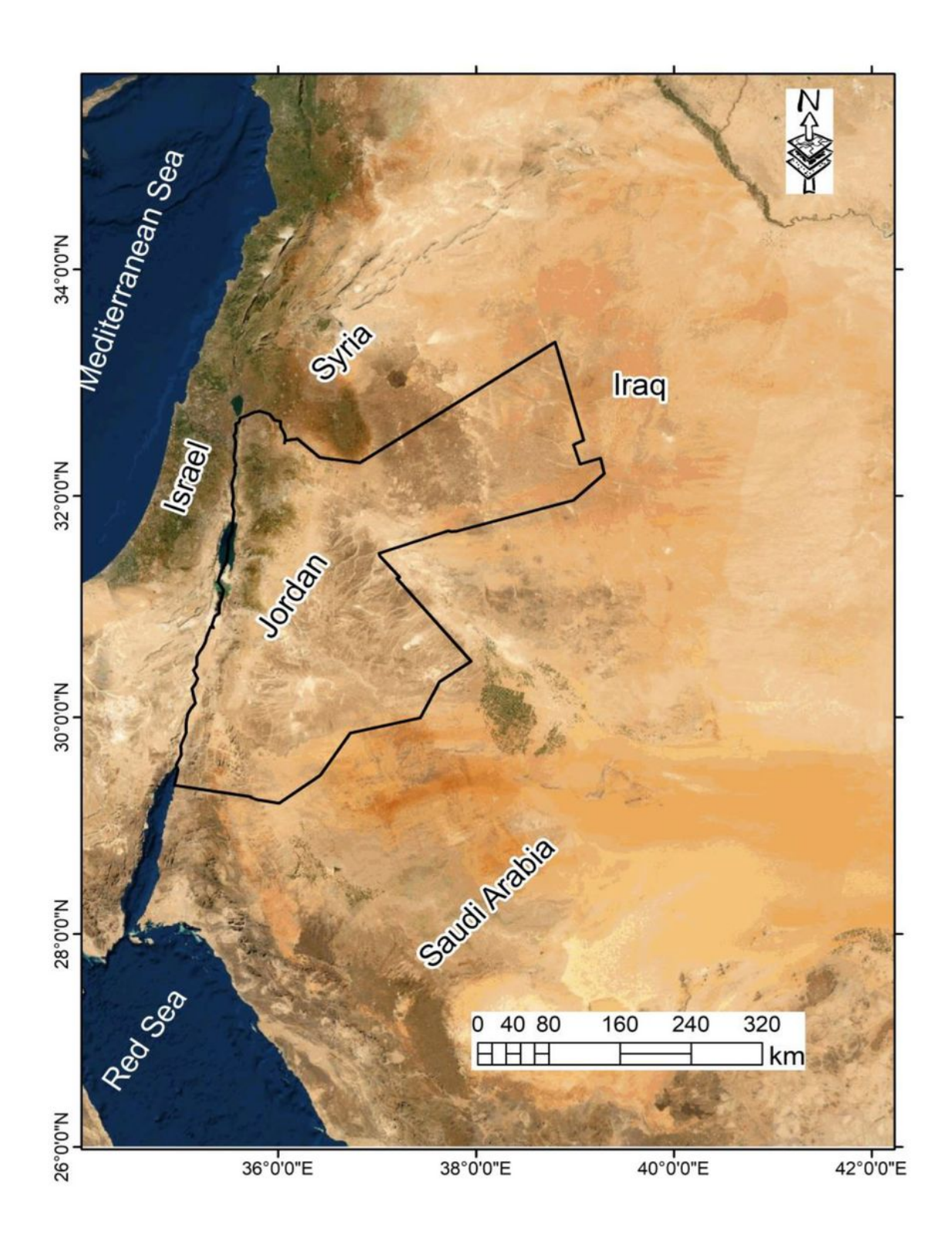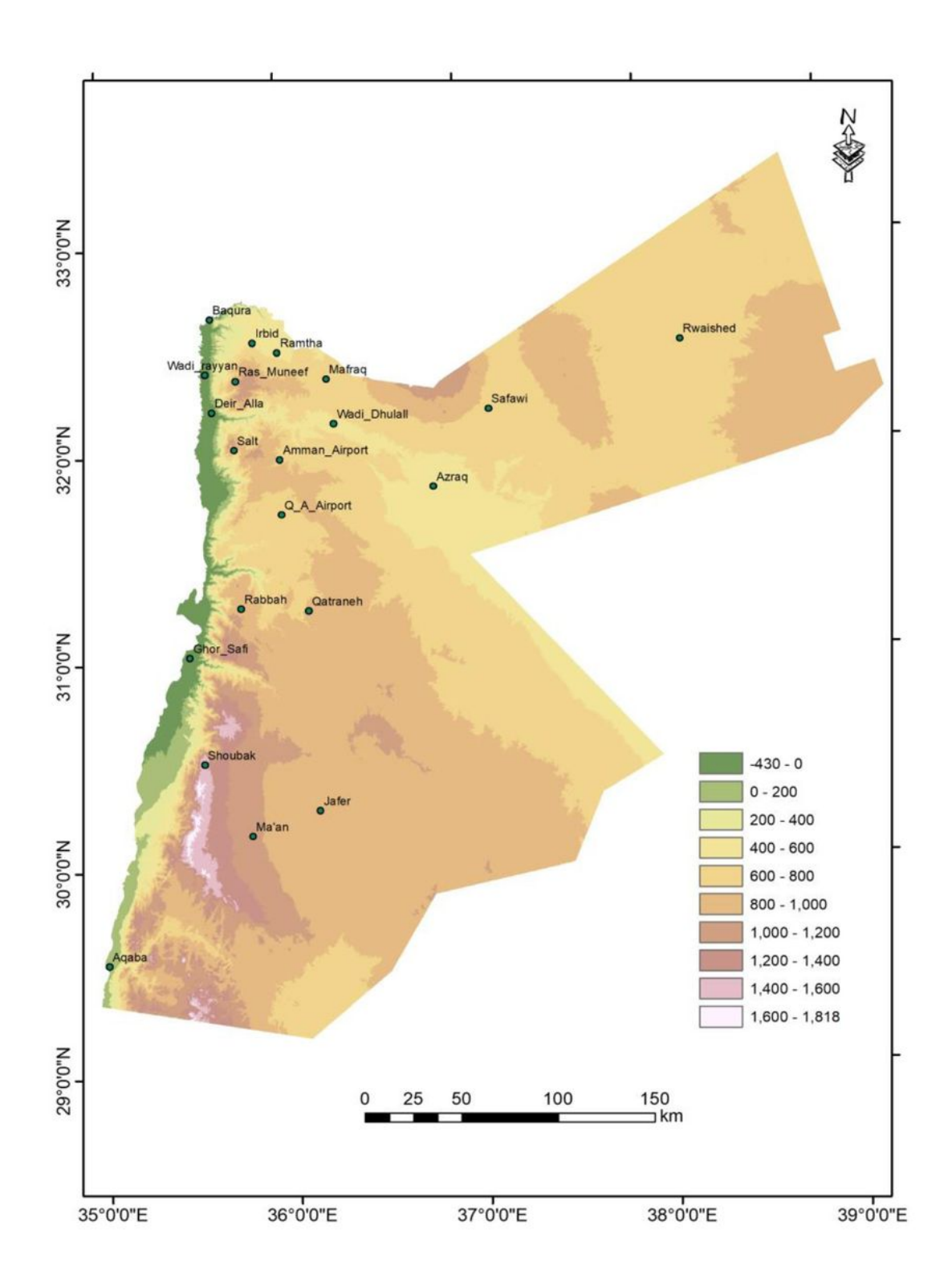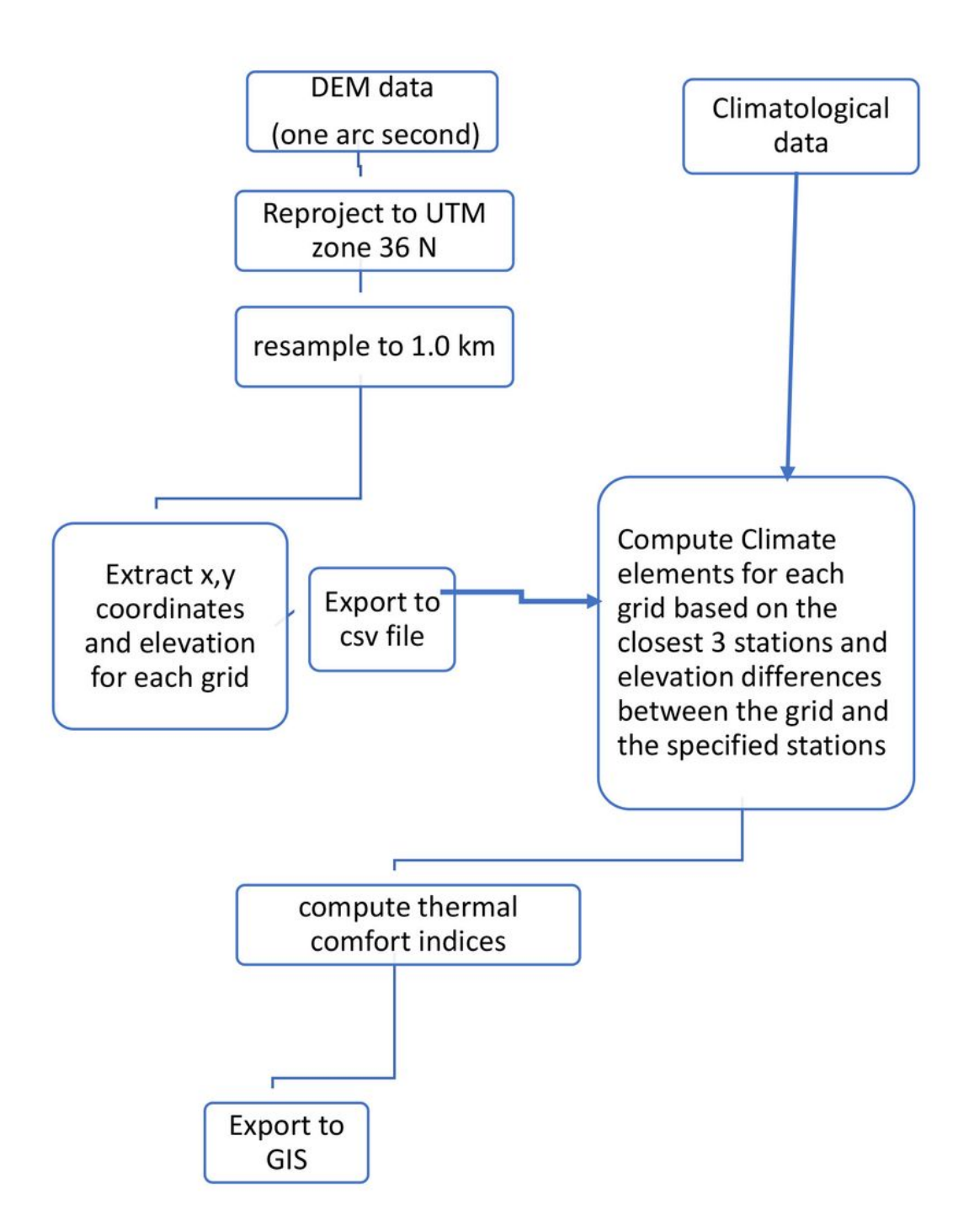
Figures

Figure 1

Location of the study area.

Figure 2

Topography of study area along with the measuring climatological stations.

Figure 3

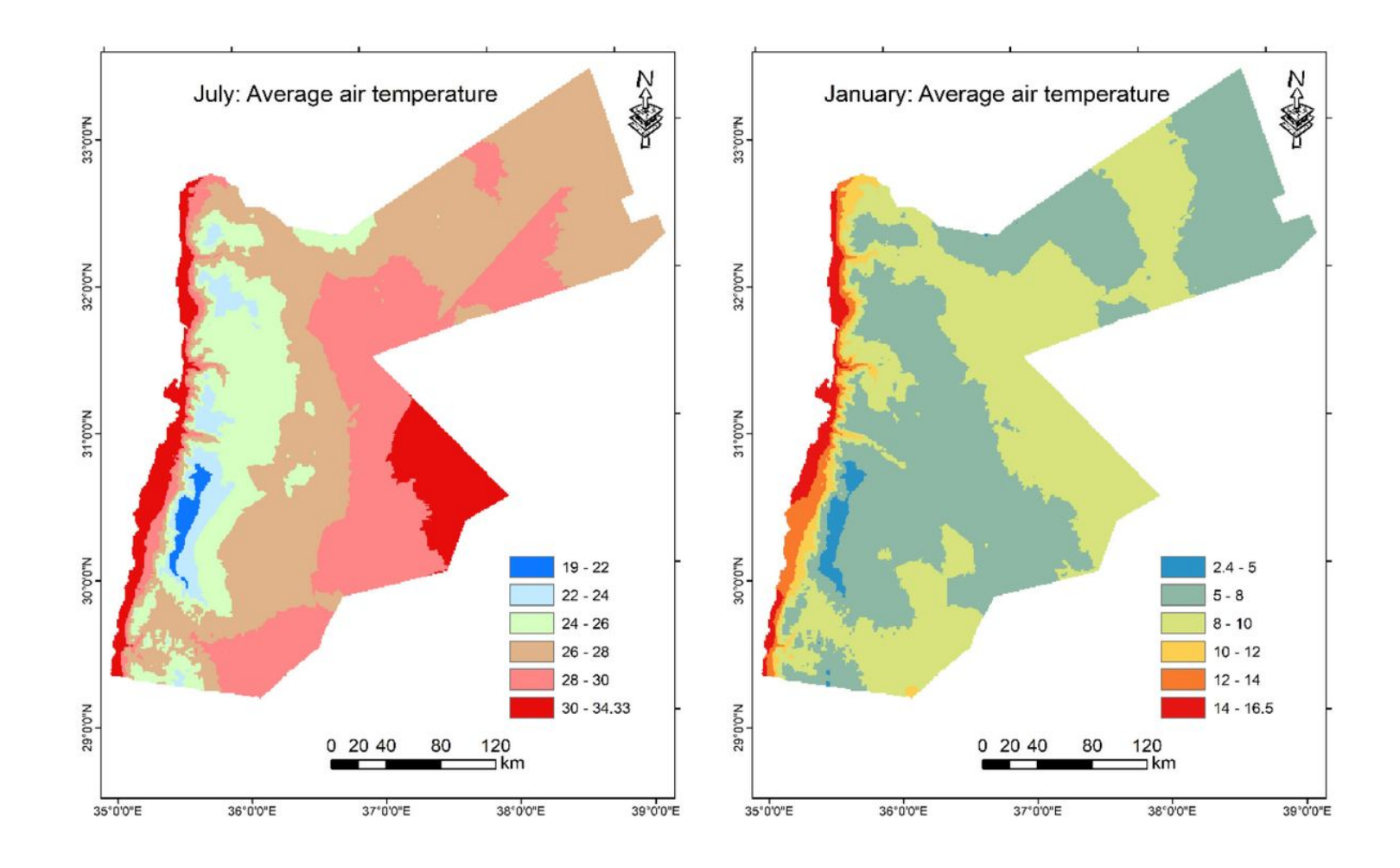Flowchart of steps used to carry out the investigation.

Figure 4

The spatial distribution of average monthly air temperature in July and January.
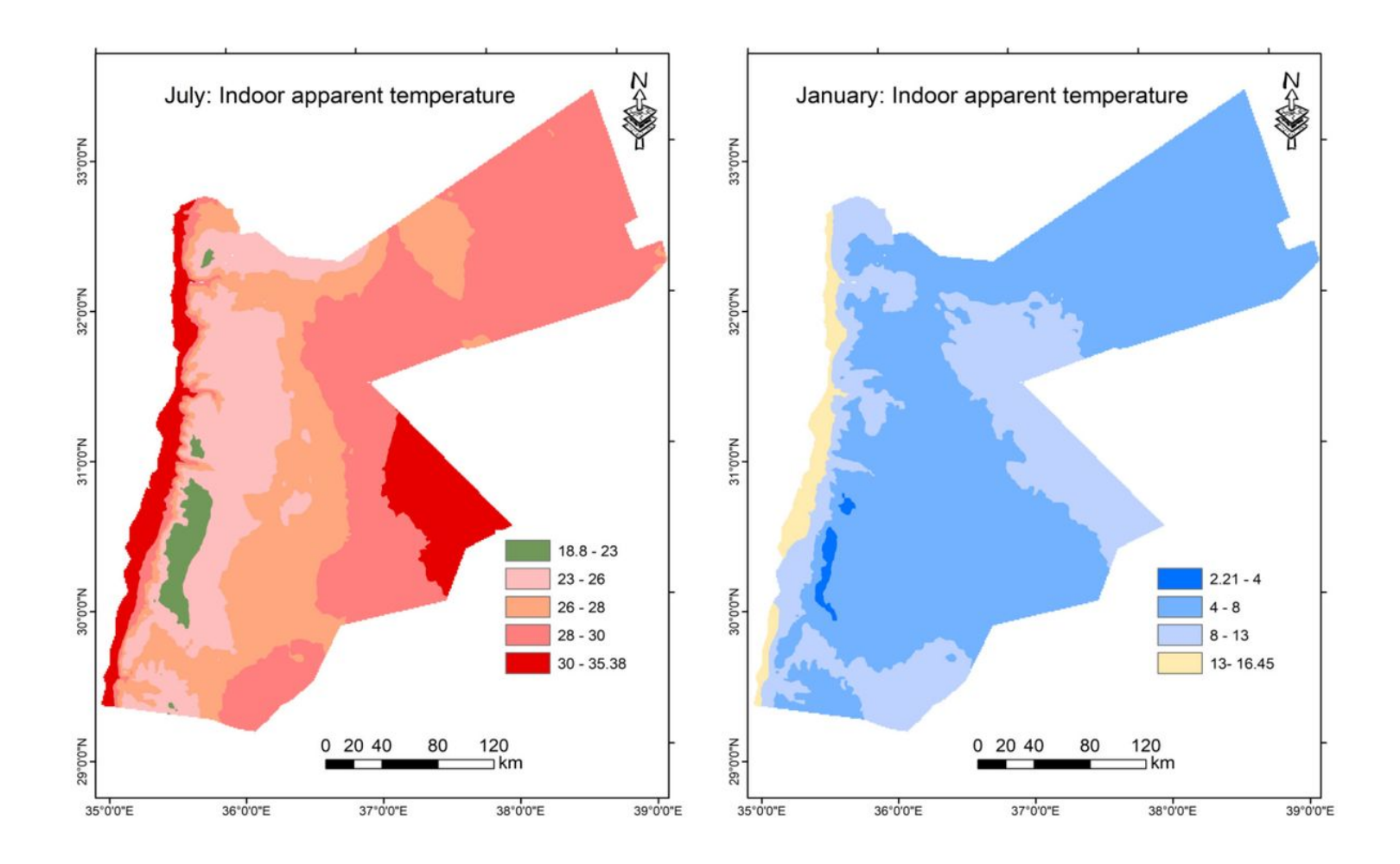
Figure 5

The spatial distribution of indoor apparent temperature in July and January.
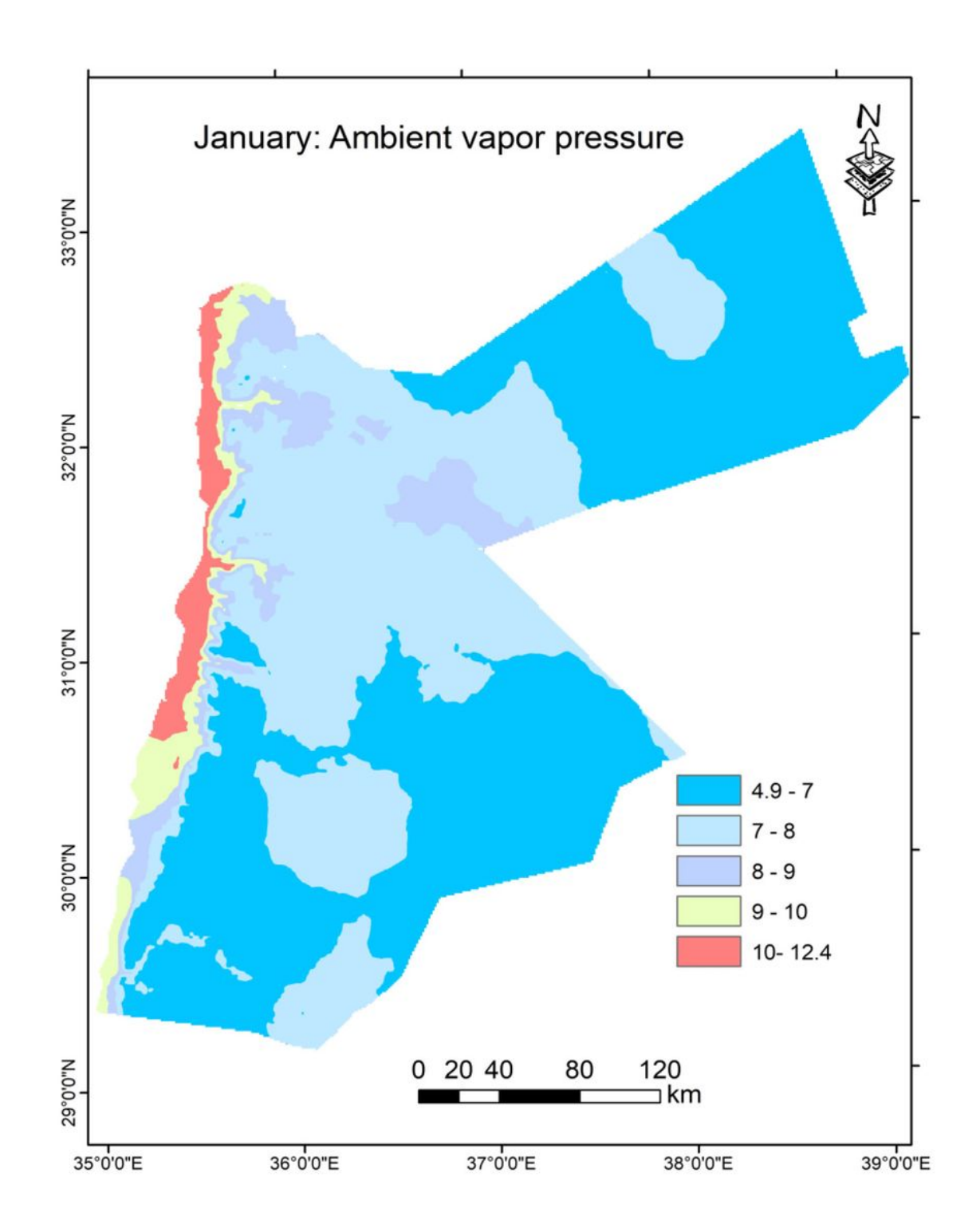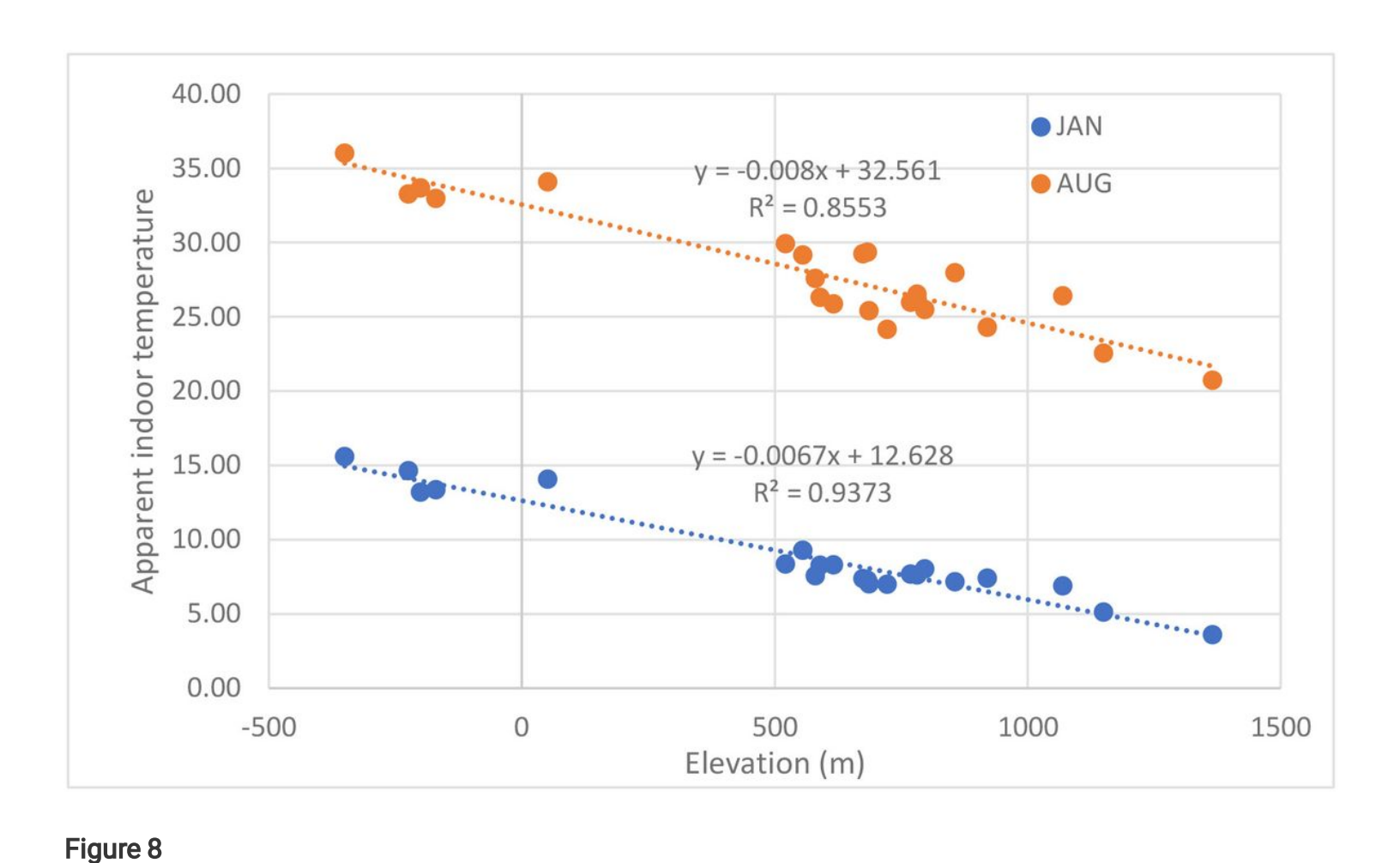
Figure 6

The spatial distribution of ambient vapor pressure across Jordan in January.

STATION	Long.	Lat.	Elev.	SEPT	OCT	NOV	DEC	JAN	FEB	MARCH	APR	MAY	JUNE	JULY	AUG
Shobak	35.53	30.5	1365	18.70	15.19	9.60	5.42	3.60	4.42	7.04	11.19	14.92	18.32	20.59	20.73
RasMunif	35.75	32.4	1150	21.44	18.64	12.34	7.37	5.12	5.47	8.31	12.99	17.44	20.61	22.52	22.56
Q_A_Airp	35.98	31.7	722	22.60	19.54	13.47	8.72	7.02	7.93	10.43	15.00	19.08	22.17	24.23	24.16
Rabbah	35.75	31.3	920	22.63	19.92	14.43	9.46	7.42	7.97	10.38	14.49	18.71	22.15	24.28	24.30
Mafraq	36.25	32.4	686	23.77	20.27	13.83	8.77	7.04	8.07	10.92	15.53	20.11	23.57	25.47	25.43
Salt	35.73	32	796	23.77	21.38	15.28	10.44	8.04	8.14	10.82	15.34	20.06	23.25	25.50	25.50
Ramtha	35.98	32.5	590	24.31	21.20	15.14	10.22	8.28	8.96	11.25	16.02	20.53	23.81	25.82	26.32
Qatraneh	36.12	31.3	768	23.78	20.25	14.14	9.42	7.69	8.46	11.33	16.20	20.42	23.56	25.82	26.00
Maan	35.78	30.2	1069	24.66	20.24	13.44	8.72	6.89	8.22	11.37	16.19	20.44	24.06	25.88	26.44
Irbid	35.85	32.6	616	24.48	21.71	15.70	10.38	8.32	9.34	11.64	15.57	20.42	24.62	25.93	25.89
AmmanA	35.98	32	781	24.73	21.41	14.78	9.53	7.64	8.47	11.12	15.53	20.27	24.19	26.42	26.54
WadDhul	36.28	32.2	580	25.71	21.48	14.27	9.15	7.57	8.84	11.93	16.71	21.48	25.19	27.45	27.60
Jaffer	36.15	30.3	856	25.96	21.25	14.17	8.85	7.17	8.73	12.19	17.37	21.87	25.41	27.50	27.97
Rwaished	38.2	32.5	683	26.92	21.90	14.32	9.07	7.27	8.87	12.40	17.38	22.29	26.53	28.99	29.37
Safawi	37.13	32.2	674	27.32	22.55	14.77	9.25	7.38	8.90	12.39	17.46	22.60	26.71	29.02	29.24
ZARKA	36.117	32.1	555	26.96	23.81	16.24	11.08	9.30	10.11	13.46	18.15	22.74	26.71	29.26	29.16
Azraq	36.82	31.8	521	27.94	23.23	15.26	9.94	8.38	9.81	13.33	18.75	23.75	27.53	29.65	29.93
Baqurah	35.62	32.7	-170	30.77	27.01	20.76	15.24	13.36	13.97	16.50	21.16	26.11	30.23	32.64	32.98
DeirAlla	35.62	32.2	-224	31.18	28.22	22.34	16.66	14.64	15.21	17.87	22.38	26.89	30.77	33.01	33.28
W_Ryan	35.58	32.4	-200	31.66	27.51	20.55	14.95	13.20	13.82	16.44	21.10	26.06	30.50	33.09	33.68
Aqaba	35	29.6	51	31.34	27.52	21.16	15.69	14.09	15.50	18.61	23.15	27.64	31.56	33.89	34.10
Ghor_Saf	35.47	31	-350	33.70	29.65	22.58	17.05	15.59	16.68	19.80	24.14	28.72	32.69	35.67	36.03

Figure 7

A scatterplot of the relationship between indoor thermal comfort and elevation.

Figure 8

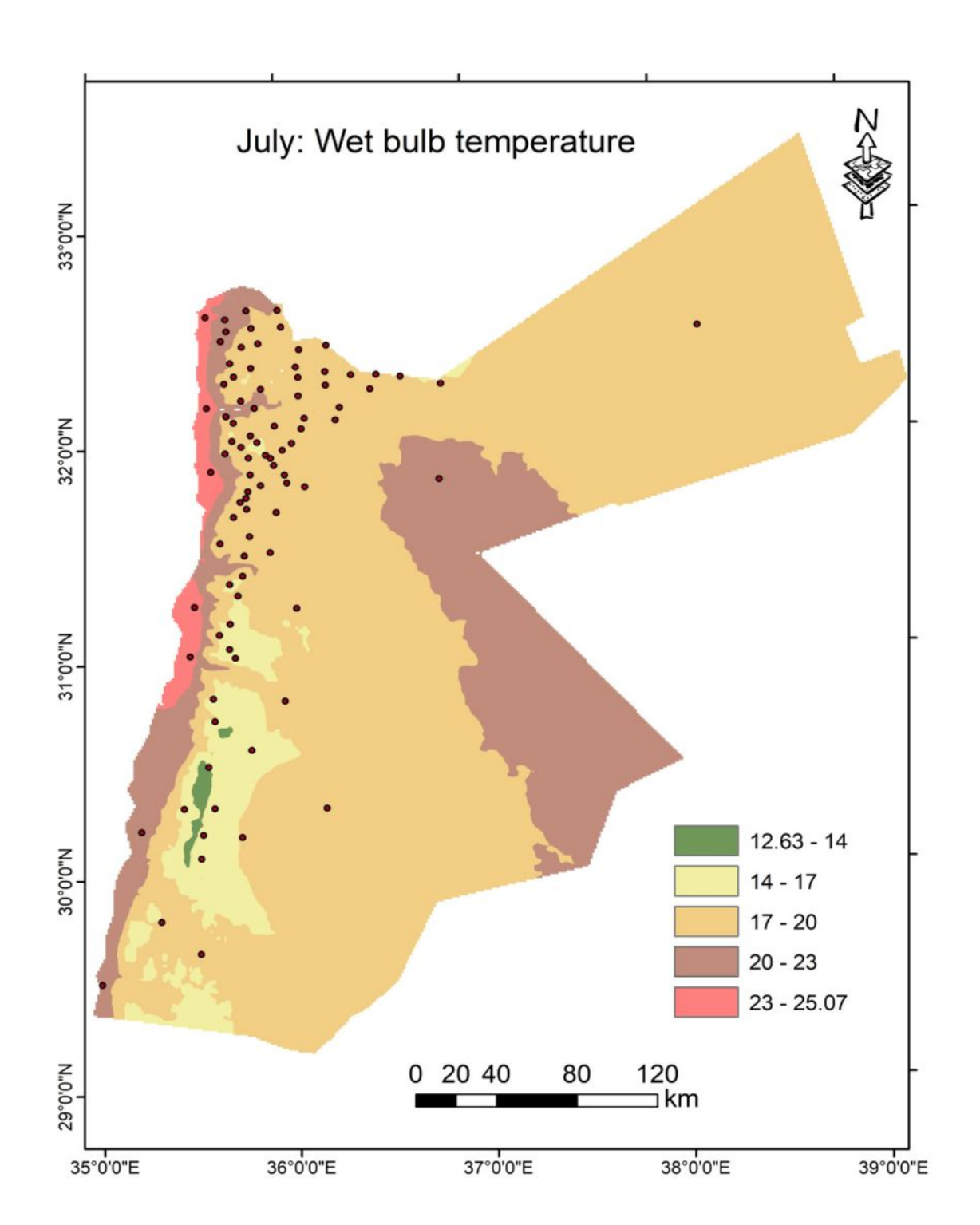The average monthly indoor apparent temperature for twenty-two locations.

Figure 9

Spatial distribution of the wet bulb temperature during July.